We are IntechOpen,
the world's leading publisher of
Open Access books
Built by scientists, for scientists

4,800

Open access books available

122,000

International authors and editors

135M

Downloads

Our authors are among the

154

Countries delivered to

TOP 1%

most cited scientists

12.2%

Contributors from top 500 universities

CLARIVATE ANALYTICS
BOOK CITATION INDEX
INDEXED

WEB OF SCIENCE™

Selection of our books indexed in the Book Citation Index
in Web of Science™ Core Collection (BKCI)

Interested in publishing with us?
Contact book.department@intechopen.com

Numbers displayed above are based on latest data collected.
For more information visit www.intechopen.com

Characterization of the Electronic Structure of Spinel Superconductor LiTi$_2$O$_4$ using Synchrotron X-ray Spectroscopy

Chi-Liang Chen and Chung-Li Dong

Additional information is available at the end of the chapter

1. Introduction

Numerous studies on high-transition temperature (T_c) superconductivity were motivated primarily by the intention to explore the nature of cuprates. Experimental results, particularly those based on hard X-ray absorption spectra, show that Cu ions reveal a mixed valence and are accountable for high-T_c superconductivity. Recently discovered iron-based superconductors with perovskite blocking layers [i.e., LnFeAsO (Ln = lanthanide), BaFe$_2$As$_2$, KFeAs, FeSe, and FeAs] have received considerable attention similar to cuprate superconductivity, which was first explored in the 1980s. New superconducting compounds and non-cuprate superconductors with magnetic elements, particularly 3d transition metals, have been widely analyzed by various scholars. Spinel LiTi$_2$O$_4$ (LTO) is a titanium (Ti)-based superconductor that is considered an exotic BCS s-wave superconductor with a T_c of ~12 K [21]. This superconductor is regarded as such because it can be described using electron–phonon interaction within the framework of the BCS model [43]. Of the more than 200 typical compounds with an AB$_2$O$_4$ normal spinel structure, in which low-valent-state cation "A" occupies the tetrahedral (8a, T$_d$) interstitial sites and high-valent-state cation "B" occupies the octahedral (16d, O$_h$) sites, only a few exhibit superconductivity, including CuV$_2$S$_4$ (T_c = 4.5 K), CuRhS$_4$ (T_c = 4.8 K), and CuRhSe$_4$ (T_c = 3.5 K). LTO is the only known spinel oxide superconductor, and it has the highest T_c among superconductors with a spinel structure. The 3d transition metals occupying the O$_h$ sites in spinel oxides may generally exhibit antiferromagnetism, ferromagnetism, and charge/orbital ordering. The nature of magnetic and electronic properties depends on the average valence of the cations. The closely related case of LiV$_2$O$_4$ (LVO), which is an isostructural compound, exhibits distinct physical properties. LVO is the closest neighbor to LTO, and it contains a mixed-valence system with an equal ratio of V^{3+} (S = 1) and V^{4+} (S = ½). LVO exhibits

strong electronic correlation, resulting in a greatly enhanced effective mass. The resistivity of this compound displays a metallic character. Although LVO is not a superconductor, it exhibits a heavy fermionic behavior typically observed in a Ce-based (4f electron) system [2, 22].

Similar to cuprates [6, 33] and pnictides [9, 24], Ti-based superconductors (titanate) present the possibility of a mixed-valence state (with electronic configuration of $3d^{0.5}$, equal ratio of Ti^{3+} of spin S = 1/2 and Ti^{4+} with S = 0) in the ground state. Given that magnetic impurities can suppress the superconductivity of various materials, an investigation into whether the dilute doping of magnetic ions in LTO results in the complete suppression of superconductivity must be conducted. Such an undertaking may provide valuable insights into the mechanism of superconductivity. A previous research observed a rapidly suppressed superconducting T_c in magnetically doped system $LiTi_{1-x}M_xO_4$ (M = Cr and V) [19]. Among the explored dopants, vanadium (V) was determined to be more effective in decreasing T_c even at small proportions, and it was also observed in other $3d$ transition metals (e.g., Cr, Mn, Fe, etc.). The results of the study not only signified the magnetic influences and other mechanisms for T_c suppression, but also the charge density wave and structural distortion. For V-doped LTO, the T_c of LTO decreases with V at 2% proportion from ~13 K to ~5 K [18, 19, 24, 49]. These superconducting activities in such a series may unravel the mechanism of superconductivity. Material study on the atomic/electronic structure has essentially illuminated the understanding of its electron transportation properties. Studies have investigated the electronic structure of LTO [8, 39]. The decrease in superconductivity of V-doped LTO is discussed based on a pair-breaking mechanism [19] and a crystalline distortion from octahedral symmetry [34]. The change of Ti and V valence states is suggested to be thoroughly linked to their chemical and physical properties. Electron–electron interaction cannot be overlooked because magnetic ions occupy the structures [32]. In this event, the mechanism of superconductivity remains unknown.

The atomic and electronic structures of the novel spinel LTO superconductors have been investigated. X-ray spectroscopy, X-ray absorption near-edge structure (XANES) spectroscopy, and resonant inelastic soft X-ray scattering (RIXS) spectroscopy are powerful tools for obtaining information on the local orbital character of a specific element. These approaches are also used to probe occupied or unoccupied electronic states near the Fermi level (E_F) and the structural symmetry of mixed-oxide systems. However, these spectroscopic techniques are sensitive to atomic symmetry because edge-sharing charge and charge distribution induce electron–electron and electron-orbital interactions, which may be related to the magnetic nature of the transition metal systems.

XANES spectroscopy is a sensitive tool that can be employed to probe unoccupied electronic states above E_F and to analyze the structural symmetry of mixed-oxide systems [10, 12]. It can provide details on the electronic–orbital interaction from the transition metal $3d$-O $2p$ hybridization states and the symmetry of the atomic structure. Therefore, the Ti L- and K-edges can be used to determine the valence states of Ti ions in $LiTi_{2-x}V_xO_4$ (LTVO). The V ions occupying and doped in the O_h site may distort the crystal structure of LTVO because of the bonding of O–Ti–O as well as the unoccupied states in the $3d$ orbitals [34].

RIXS spectroscopic technique is used to explore the electronic structure of materials and to associate the structure with the XANES spectrum. RIXS is a process that describes the de-

excitation of the final state of X-ray absorption, providing information on ground state via the excited intermediate states. Consequently, by tuning various excitation energies, certain RIXS features can be enhanced, allowing the separation of different electronic configurations in the mixed ground states [11, 30, 42]. The above conditions indicate that RIXS is a complementary tool compared with XANES. Unlike XANES, RIXS can be used to investigate a forbidden electronic transition (e.g., *d-d* or *f-f* excitation) because it involves two dipole-allowed transitions, given that its final state has symmetry similar to that of the initial state of the former. The RIXS of TM L-edge can reflect the 3*d* partial density of states and is regarded as a useful approach for analyzing the electron correlation among strongly correlated materials [31, 36, 45] as well as the charge transfer between TM 3*d* and O 2*p* orbitals.

In this research, XANES and RIXS spectra were applied to understand the influence of V doping on the atomic/electronic properties of the LTVO system and to discuss the basis of the quick suppression of superconductivity. The occupied or unoccupied states near E_F of a solid-state solution may be a useful starting point in obtaining fundamental information on the complicated behavior of materials, including ferrites, high-T_c superconductors, and strongly correlated and ladder systems. These properties demonstrate that magnetic behavior and atypical physical and chemical characteristics can be synthesized and analyzed. The obtained X-ray spectra reveal that the rapidly suppressed superconductivity is associated with the variation of Ti-O hybridization mainly at e_g bands rather than with the magnetic nature of the substituted V ion.

2. Experiments

All the LTVO samples were synthesized through conventional two-step solid-state reactions with highly pure oxides of TiO$_2$ (99%), Li$_2$CO$_3$ (99.99%), and V$_2$O$_3$ (99%) [19]. The samples were dried at 150 °C for at least 2 h. Additional Li$_2$CO$_3$ (5 mol%) was added into the samples to compensate for lithium evaporation at high temperature. These processes were performed in a dynamic vacuum environment. In the first step, a mixture of Li$_2$CO$_3$ and TiO$_2$ was pulverized and calcined at 750 °C for 8 h in ambient air. The mixture was pulverized and calcined again at 800 °C for 12 h to form the intermediate compound Li$_2$Ti$_2$O$_5$. In the second step, the stoichiometric powders of Li$_2$Ti$_2$O$_5$, Ti$_2$O$_3$, and V$_2$O$_3$ were mixed and ground and then cold-pressed into pellets. The pellets were wrapped with gold foil and sintered in an alumina crucible at 880 °C for 24 h in a dynamic vacuum environment at less than 10^{-5} torr. The final products were stored in an Ar-filled glove box or vacuum desiccator to prevent aging. Powder X-ray diffraction (XRD) patterns [19] with X-ray (Cu, K$_\alpha$ =1.5418 Å) radiation in a diffractometer (Philips PW3040/60) confirmed the phase purity of the product and showed the variation of the lattice parameter as a function of V dopant. Different proportions of the dopant up to 2% were selected to understand the effect of dilute doping. Oxygen stoichiometry was expected to remain constant for all small concentrations given that the preparations were all the same.

XANES spectra were obtained from the National Synchrotron Radiation Research Center (Taiwan) and were operated at 1.5 GeV with a current of 360 mA. The K-edge of Ti and V K-

edge of LTVO were measured with a wiggler beamline BL17C1 equipped with Si (111) crystal monochromators. The absorption spectra were recorded in the fluorescence-yield mode with a Lytle detector [27]. These hard X-ray absorption spectra, which could provide information on the unoccupied states with transition metal p state, were normalized to a unit step height in the absorption coefficient from below to above the edges. The oxide powders, namely, TiO_2, VO_2, Ti_2O_3, and V_2O_3, and standard metal foils were used for energy calibration and for comparing the electronic valence states. The XANES spectra at the Ti L- and O K-edges were determined at beamline BL20A in the total-electron-yield mode using an ultrahigh-vacuum chamber with pressure of ~5×10^{-9} torr. All spectra were normalized with the standard procedure.

The experiments for X-ray emission spectroscopy (XES) were conducted at beamline 7.0.1 at the Advanced Light Source, Lawrence Berkeley National Laboratory. The beamline is armed with a spherical grating monochromator and an undulator (period 5 cm in 99 poles) [3]. The RIXS spectra were recorded with a high-resolution grating spectrometer at grazing incidence with a 2D detector [17]. The resolution for Ti L emission spectra was about 0.4 eV. The monochromator resolution was set up similar to that of the emission measurements.

X-ray absorption at the Ti L-edge determined that the electron in the Ti 2p core level was excited to the unoccupied Ti 3d and 4s orbitals. XES recorded the signal from the decay process related to the partial densities of Ti 4s and 3d states. RIXS spectra were acquired by tuning different excitation energies according to the x-ray absorption spectral profile to measure XES. Sample current mode was employed to record XANES with an energy resolution of ~0.15 eV. Meanwhile, a high-resolution grazing-incidence grating spectrometer with a 2D multi-channel plate detector was used to record XES at a resolution of 0.6 eV [36].

3. Results and discussion

3.1. Structure of LTVO

The crystal structure of cubic spinel LTO, which belongs to the Fd3m space group, is illustrated in Fig. 1(a). The structure demonstrates that the lattice parameter of LTO is 8.404 Å (a = b = c) and contains eight AB_2O_4 units per unit cell. In general, a spinel structure has a total of 56 ions, 32 anions, and 24 cations per unit cell. The Li, Ti, and oxide ions are located at tetrahedral (T_d) A-sites, octahedral (O_h) B-sites, and 32e sites, respectively. The XRD patterns of $LiTi_{2-x}V_xO_4$ (x = 0, 0.05, 0.01, 0.015, and 0.02) are shown in Fig. 2(a). The result of the chemical analysis (determined with ICP-AES) is consistent with the nominal composition [19, 18, 24, 49]. These patterns reflect that the crystal structure is of pure spinel structure without an impure phase. The lattice parameter of LTVO samples displayed in Fig. 2(b) linearly decreases with the increasing concentration of the dopant. Doping V, which has a smaller ionic radius, induces a change in the lattice parameter when in a Ti site. This lattice shrinkage can be attributed to the fact that the ionic radius of V^{3+} (0.64 Å) is smaller than that of Ti^{3+} (0.67 Å) in the O_h site [29]. The rate of shrinkage of the lattice parameter is ~3.6 Å/at% based on the occupancy of O_h sites. This rate is also related to the bond length between the cations (Ti and V) and oxygen. Electronic

structure strongly depends on the hybridization states of the transition metal 3d-O 2p orbitals nearby E$_F$ when electronic exchange normally occurs. Thus, the changed electronic structure around the transition metal ions greatly affects the oxidation state and physical properties of the latter. Considering these physical properties in AB$_2$O$_4$ with mixed-valence states require wide-ranging knowledge of their electronic structure, particularly the p-d hybridization and spin-orbital symmetry. Several experiments and theories show that AB$_2$O$_4$ exhibits strong electron–hole correlations because of the TM ions located in various sites [8, 39].
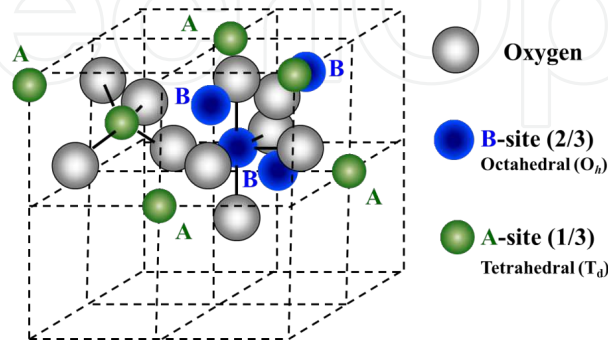

Figure 1. Crystal structure of LTO [Li (green), Ti (blue), and O (grey)].
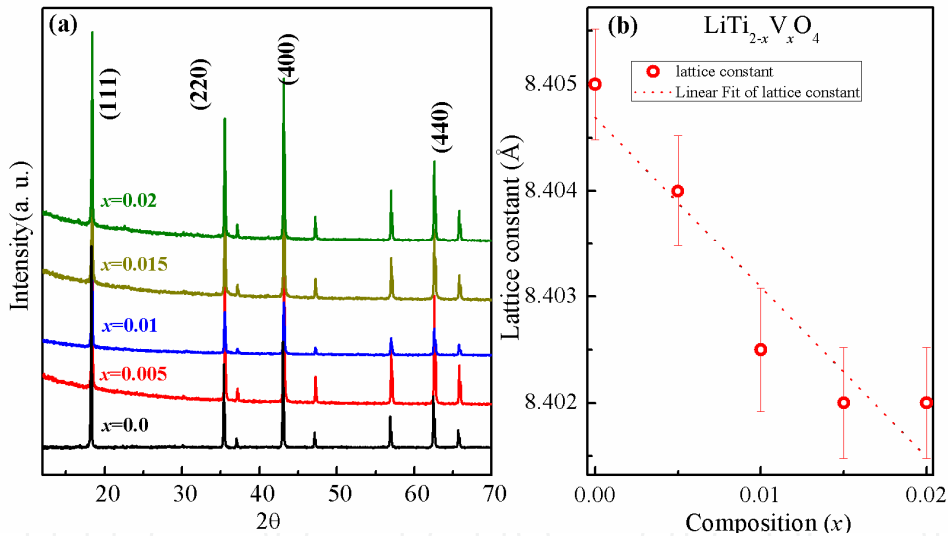

Figure 2. (a) Powder XRD patterns of LTVO crystals with x = 0, 0.005, 0.01, 0.015, and 0.02. The patterns are fitted to the Fd3m space group and are indexed. (b) Chemical composition of V dependence of the lattice constant of LTVO.

3.2. Resistive properties

The transport properties of the samples are specified in Fig. 3(a) with V doping of less than 0.025. The findings indicate that the superconducting T_c is suppressed with an increasing proportion of the dopant. Fig. 3(c) reveals that the resistivity of the samples gradually increases. The un-doped LTO has a superconducting T_c of ~12 K with a transition width ($\triangle T_c$) of ~0.4 K. Fig. 3(b) indicates that when the Ti ion is replaced with V ions, T_c exhibits an abrupt but linear suppression with respect to the level of doping. Given the magnetic pair-breaking effects [47],

the doped magnetic ions suppress superconductivity. Considerable research has been devoted to exploring cuprate [48]; Tarascon et al., 1987) and pnictide [41] superconducting systems based on resistivity measurements. For the LTO series, the effect of doping with both non-magnetic and magnetic impurities at both T_d and O_h sites on $(Li_{1-x}A_x)(Ti_{2-y}B_y)O_4$ [A = Mg and Mn; B = Al and Cr] compounds has been previously reported [26]. The substitution of non-magnetic ions (e.g., Mg^{2+} at the T_d site and Al^{3+} at the O_h site) slightly suppresses superconductivity similar to the case when Li^+ ions occupy the T_d site. However, the effect of superconductivity suppression is greater when the magnetic Mn^{2+} ions occupy the T_d site. The suppression of superconductivity is attributed to pair-breaking when the Cooper pairs are scattered with magnetic impurities. The effect of substituting Ti^{3+} with Cr^{3+} at the O_h site is even more significant.
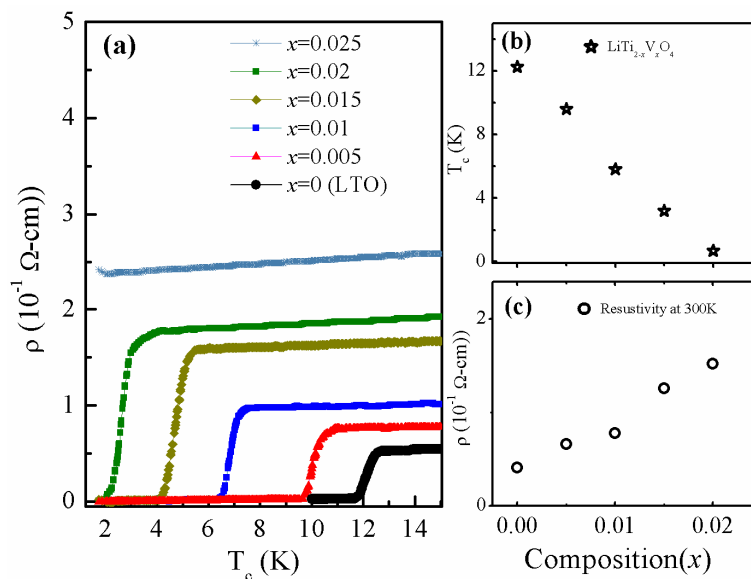

Figure 3. (a) Transport properties of LTO and LTVO samples at low temperature without magnetic field. (b) Chemical composition of V-dependence of superconducting T_c. (c) Resistivity at room temperature.

The resistivity near 300 K increases as x increases [Fig. 3(c)], indicating the extreme sensitivity of the transport properties to the electronic effect of $3d$ transition metals. The itinerant carrier density can be attributed to the cation (Ti^{3+}) in LTO. Similar to the reports of a previous study on Al-doped LTO [16], the results of the current study clarify the effect of carrier density on superconductivity, such that the resistivity increases with the level of doping in the normal state. Except for the semiconducting behavior at the normal state, a similar T_c has been determined in $LiTi_{1.7}$, $Al_{0.3}O_4$, and LTO samples [19]. This observation implies that T_c is slightly affected by substituting a considerable proportion of the trivalent non-magnetic ions. The ratio Ti^{4+}/Ti^{3+} in O_h symmetry can then be modulated with impurity doping to vary the superconducting properties of LTO. Electron–electron interaction may be a key factor in causing changes in the transport properties of the samples. By distorting the local symmetry of the spinel structure, V substitution will not only alter the valence of Ti, but the hole/electron effect as well. This phenomenon is discussed in the next section.

### 3.3. Electronic structure results based on x-ray spectra

With the aim to investigate the effects of V dilute doping on LTO, this research measures XANES and RIXS at Ti L-edges. As shown in the inset in Fig. 4(a), the Ti L-edge XANES spectra exhibit several well-resolved features because of the excitations of a 2p core electron into the Ti 3d empty states, that is, a transition from the ground state with configuration $2p^63d^n$ to an excited electronic configuration $2p^53d^{n+1}$ with numerous multiplet excitations. When the spin-orbital coupling is in the transition metal 2p state, the spectra reveal two prominent features located at the energy ranges of 455 eV to 461 eV and 461.2 eV to 468 eV, corresponding to the absorptions L$_3$ ($2p_{3/2} \rightarrow 3d$) and L$_2$ ($2p_{1/2} \rightarrow 3d$) edge respectively. These prominent features are due to a strong Coulombic interaction between the poorly screened Ti 3d electrons and the Ti 2p core hole [12]. L_2 edge features are normally broadened compared with the L$_3$ edge because of the lesser lifetime of the $2p_{1/2}$ core hole (i.e., a radiationless electron transition from energy level $2p_{3/2}$ to the $2p_{1/2}$), accompanied by the promotion of a valence electron into the unoccupied states (conduction band). In the O$_h$ crystal field, the 3d band splits into t_{2g} (d_{xy}, d_{xz}, and d_{yz}) and e_g ($d_{x^2-y^2}$ and $3d_{3z^2-r^2}$) subbands [$\Delta = (e_g) - (t_{2g}) = 10$ Dq]. Given the O$_h$ crystal-field splitting, the Ti L$_3$-edge feature possesses t_{2g} and e_g bands. The RIXS Ti 3d spectra of LTO and doped LTO (V 2 %) are exhibited with energy-loss scales in Fig. 4(a). Four distinct spectral features are observed in RIXS spectra. These features are as follows: elastic peak at the energy loss at zero, d–d excitations at about 4 eV, a broad-band feature at around 7 eV, and a large energy dispersed-feature above 10 eV. Letters a to k denote the different exciting energies based on the XANES spectra, as displayed in the inset of Fig. 4(a). For example, XES spectrum b is collected by tuning the incident photon energy at 457 eV in XANES. The inelastic scattering features ranging from 5 eV to 10 eV originate from the complicated charge-transfer excitation from O 2p to Ti 3d t_{2g} and e_g subbands [1, 31]. The low-energy inelastic scattering features absent in TiO$_2$ are observed at energy of less than 5 eV [36]. The spectra within this energy range significantly differ from that of TiO$_2$. The appearance of Ti^{3+} implies that an electron occupies the empty 3d t_{2g} orbitals, thus inducing the energy-loss features. Strong d-electron correlation is revealed because the relative intensities of peaks A$_4$ and B$_4$ (d-d excitations) are observed to be markedly different at varying excitation energies. An enhanced energy-loss peak is observed at 1 eV in spectrum a, and the intensity of this peak intensively drops when the excitation energy is tuned to a higher energy (peak b in XANES). With the increase of excitation energy at c, another intense peak at energy loss of about 2.9 eV is observed. An excitation energy tuned below the L$_3$ t_{2g} peak in the spectrum (letter a) enhances inelastic scattering A$_4$, which is uncommon. This enhanced inelasticity is not observed at either t_{2g} (b) or e_g (d) resonant energy. This phenomenon can be explained by considering the presence of Ti^{3+}, as revealed by the constant-initial-state absorption spectrum [3]. The spectral shapes in XANES spectra are similar for both LTO and LTVO, wherein spectral differences are slightly small. Given that the spectral change of XANES is small with V doping, the spectral deconvolution and specific electronic state can be measured separately from RIXS [11]. The result at a specific energy (c) in Figs. 4(b) and 4(c) indicates that an enhanced trivalent Ti contribution is observed at a dip quadrivalence within the spectrum (between t_{2g} and e_g). The Ti^{3+} t_{2g}- and e_g-resonance energies correspond to the excitation energies 456 and 457.5 eV respectively. [3].
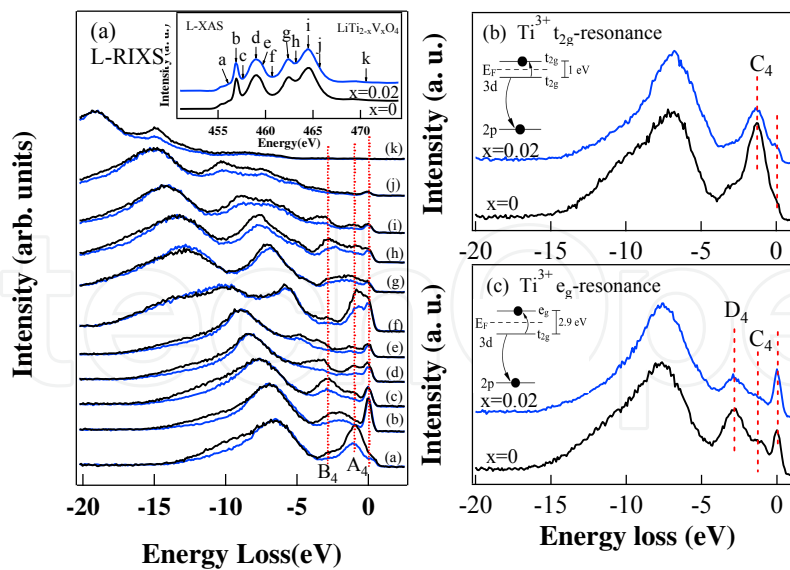
Figure 4. (a) Ti L-RIXS spectra of LTVO ($x = 0$ and 0.02) recorded with several excitation energies labeled with letters *a* to *k* in the Ti XANES L-edge spectrum. Ti L_3 RIXS spectra at (b) Ti^{3+} t_{2g}-resonance and at (c) Ti^{3+} e_g-resonance. The insets of (b) and (c) display the energy diagram of the *d-d* excitation.

When excitation energy is tuned to the t_{2g} resonance, the low-energy-excited feature C_4 at ~1 eV demonstrated in Figs. 4(b) and 4(c) is resonantly enhanced. This feature corresponds to the electron–hole pairs within the t_{2g} band. When the spectrum is acquired with energy at about e_g resonance energy [Fig. 4(c)], the intensity of peak D_4 increases. Such an increase can be attributed to the transition between the occupied t_{2g} and the unoccupied e_g states. The presence of this RIXS feature indicates a strong electron–electron association. The *d-d* excitation peak at an energy loss of about 2.9 eV corresponds to the crystal-field splitting (i.e., 10 Dq) and refers to the ground state without the core hole. The comparison of the spectra of each set shows that the intensity of the loss feature decreases with the increasing concentration of dopant ($x = 0.02$). Hence, fewer electrons are distributed in the t_{2g} band. In a previous study on TiO_2 [31], no obvious feature was exhibited in the region located below the elastic signal (peak). The change in intensity is due to the variation of the incompletely filled t_{2g} band arising from the V doped effect. This result forcefully indicates that the Ti valence is enhanced when V is doped. The active Ti ions in LTO have a formal oxidation state trivalence and quadrivalence, which display nearly 0.5 electrons in the $3d$ orbital, and possess a lesser electronic density. Doping with V reduces the number of Ti $3d$ electrons, suggesting an increase in the formal oxidation number of the Ti ion. The Ti ions show a mixed-valence state and contain some t_{2g} electrons in LTO. With no t_{2g} electron, *d-d* excitation is absent because no electron subsists in t_{2g} to be excited to the t_{2g}/e_g unoccupied state. A little variation in valence of Ti is then reflected in the RIXS spectra. The diminution or absence of features in the energy range from 0 eV to 5 eV indicates a decrease in *d–d* transitions. More electrons occupy the t_{2g} orbital when the oxidation number of Ti changes from trivalence to quadrivalence. The probability of exciting the t_{2g} electron into the unoccupied states (t_{2g} or e_g) is therefore increased. Only RIXS can observe the *d-d* excitations (t_{2g}-t_{2g} and t_{2g}-e_g) in the spectra. The significance of observing this *d-d* excitation is that the t_{2g} occupation number changes with V doping, whereas the number of t_{2g} electrons decreases with V doping. Therefore, the significant RIXS spectrum can observe this kind of valence change.
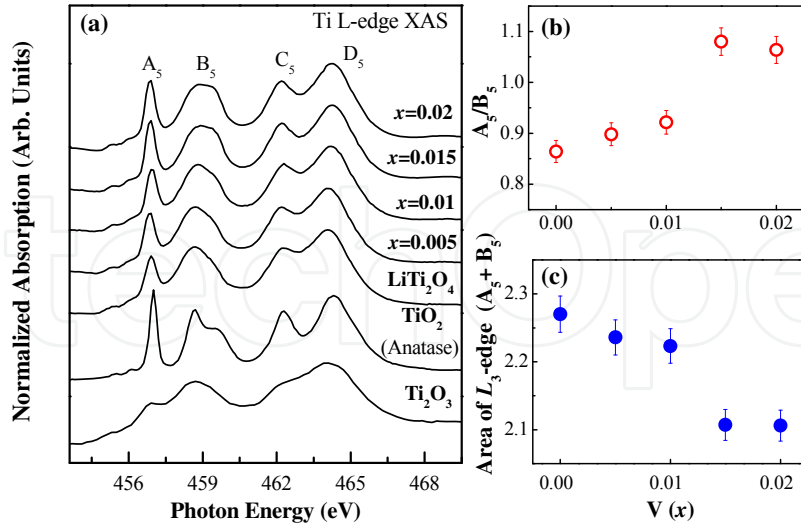
Figure 5. (a) XANES Ti L$_{3,2}$-edge spectra for LTVO (x = 0.005 to 0.02), LTO (x = 0), Ti$_2$O$_3$, and anatase TiO$_2$. (b) Integrated area ratio of A$_5$/B$_5$. This ratio increase implies the presence of 3d^0 states. (c) Total area of L$_3$-edge (A$_5$+B$_5$) decreases with the increase of V concentration

Complementary information is also acquired for this research by thoroughly analyzing the XANES Ti L$_{3,2}$-edge spectra. The spectra of LiTi$_{2-x}$V$_x$O$_4$ (or LTVO) (x = 0 to 0.02) are presented in Fig. 5(a). The white line shapes of the spectra of LTO (undoped) and slight V doping (x = 0.005) in LTO are similar. The A$_5$ and C$_5$ features (B$_5$ and D$_5$) are previously assigned as the t_{2g} (e_g) states of the 10 Dq crystal-field-split in 3d orbitals. This O$_h$ crystal-field splitting is ~1.8 eV at LTO, but increases from 1.8 eV to 2.0 eV when the V concentration increases from x = 0.005 to x = 0.02. This phenomenon reveals the distortion of O$_h$ symmetry when Ti is replaced with slight V doping. This finding is consistent with the powder XRD results and the theoretical calculations [12, 13, 15]. Moreover, the results specify that B$_5$ peak broadens with its gradual V doping. As previously reported [12, 13, 15], and according to the Jahn-Teller distortion with ΔE_{J-T} energy splitting in the e_g band, the e_g orbitals point directly toward the Ti 2p orbitals of the octahedrally coordinated O atoms. In general, e_g band is sensitive to the local environment, producing a changed bonding distance and a O–Ti–O angle in the presence of V doping. These e_g-related peaks are also broader than the t_{2g} peak because of the larger hybridization between e_g orbitals and O ligand states, and because of the associated effects of solid-state broadening [12]. The e_g feature appears as a narrow and symmetric profile in LTO, representing symmetric octahedrally coordinated Ti–O bonds. This feature becomes broad and asymmetric upon doping, suggesting a distortion. In particular, distortion may arise from the uneven Ti-O bonds in the O$_h$ symmetry. The e_g peak at the side with greater energy originates from the short Ti-O bonds because of the increase in hybridization (relative to the long Ti-O bonds); hence, the intensity ratio of the high-energy to low-energy e_g peaks is increased with V doping. This result implies that long Ti–O bonds become shorter [17]. An enhancement in the integrated area under A$_5$ peak implies the increase in unoccupied states of Ti 3d states, thereby indicating that the Ti valence increases with slight V doping. From the Ti–O bond, the electronic configuration of Ti exhibits a combination of 3d^0 ($t_{2g}^0e_g^0$) and 3d^1 ($t_{2g}^1e_g^0$) in the ground state. Fig. 5(b) shows

the integrated area of ratio A_5/B_5, which clearly increases with V doping. Consequently, the more intense A_5 (t_{2g}) feature implies a higher oxidation number and exhibits the presence of Ti^{4+} ($3d^0$) [28, 40]. Moreover, the area of the L_3-edge that corresponds to (A_5+B_5) progressively decreases when V concentration increases [Fig. 5(c)] because V replaces Ti. This trend is in good agreement with the XRD results [18]. A small but actual increase in Ti valence with slight V doping is observed in XANES Ti $L_{3,2}$-edge spectra. Such an increase is significantly obvious in the Ti L-RIXS spectra.

The pre-edge features of Ti K-edge XANES spectra are displayed in Fig. 6(a). These spectral features at K-edge are due to the transitions from the Ti $1s$ core level to the $4p$-derived final states based on the dipole selection rule. The pre-edge features are a combination of strongly hybridized Ti $4sp$ and $3d$ and O $2p$ orbitals. Quadrupole-allowed transitions generally occur at the pre-edge region in the transition metal oxides, which correspond to the contribution from $3d$ orbitals through $4sp$-$3d$ hybridization [14, 25, 37]. The inset of Fig. 6(a) reveals that a Gaussian function is subtracted from the original Ti K-edge spectrum for a detailed comparison of the pre-edge spectra. Fig. 4(a) shows the Ti K-edge spectra of LTO and LTVO (0.005 to 0.02). As marked by the black arrow in Fig. 6(a), the spectra of LTVO with a small concentration of x from 0.005 to 0.01 are similar to that of LTO with the same photon energy at the main peak A_6. The Ti valence performs to maintain +3.5 owing to the smaller concentration of V doping. Nevertheless, the intensity of the pre-peak spectrum increases relative to that of pure LTO as the doping level is increased to $x = 0.015$ and $x = 0.02$. Meanwhile, as directed by the red arrow in Fig. 6(a), chemical shift is also observed as V concentration increases. Fig. 6(b) displays the pre-edge region between 4969 and 4977 eV, as well as the three main features (i.e., C_6, D_6, and E_6) in XANES Ti K-edge spectra of TiO_2 (anatase, Ti^{4+}) and LTVO ($x = 0$, 0.02) samples. The origin of the splitting of pre-peaks is caused by local excitations ($1s$ to $3d$ t_{2g} and e_g) [5, 14, 38, 46]. Conversely, the greatest contribution to this splitting is suggested to be the corner- and edge-sharing Ti octahedra that yield non-local, intersite hybrid excitations. The next-nearest neighbor $3d$ states (t_{2g} and e_g) are related Ti $4p$ states that absorb atom via the anion O $2p$ states [7, 23, 44]. The local structure of Ti for LTO and LTVO also possesses O_h symmetry; hence, the pre-peak region (A_6 and B_6) can be described in terms of a similar scenario [23, 44, 7]. The intensity of these pre-peaks varies with V concentration. In the V-doped LTO, the substitution of V for Ti slightly decreases the lattice parameter [18]. A reduced bond length (Ti–O–Ti) subsequently increases the overlap of the first-nearest-neighbors and the absorbing atom (e.g., Ti $4p$-Ti $3d$ orbitals) mediated by O ion. Therefore, these pre-peaks are closely related to the increase in the number of the first-nearest-neighbor unoccupying the Ti $3d$ states. These intersite hybrid peaks intensities increase with the increase of V concentration. The inset of Fig. 6(b) shows that the variation in the area under the pre-peak suggests that the $3d$ unoccupied states are altered via the interaction of the Ti $4p$-O $2p$-Ti $3d$ states. These results strengthen the conclusion that Ti is in mixed-valence states between LTO and LTVO [14, 24]. The analysis of the spectra of LTO and LTVO ($x = 0.02$) reveals that pre-peaks A_6 and B_6 are stronger in LTVO than in LTO, attended by a chemical shift of the main peak to higher energy. Therefore, Ti valence is increased when V is doped. The average valence of Ti in the case of doped LTVO ($x = 0.015$ and 0.02) is approximately +3.6, which is obtained with a simple calculation and a fit of the ratio of areas under the spectral lines.

The O K-edge XANES spectra [Fig. 6(c)] provide useful information about the unoccupied density of states in TMO because of the covalent mixing between O and TM ions. The two pre-edge features are at about 530 eV to 536 eV because of the strong hybridizations in Ti 3d–O 2p states, and correspond to the t_{2g} and e_g states of Ti 3d orbitals respectively. The intensity of the t_{2g} and e_g peaks at the O K-edge changes is similar to an increased peak ratio t_{2g}/e_g in Ti L-edge XANES. In sum, the above results specified by the XANES and RIXS spectra strongly confirm that the valence of Ti is increased when the doping level of x increases. Thus, the Ti-O hybridization and electron–electron correlation are modified when a slight doping of V ions completely suppresses the superconductivity of LTO.

Previous studies have indicated that LTO is a spinel superconductor, whereas spinel LVO reveals a heavy fermionic behavior with a Curie-Weiss spin susceptibility and a large electronic specific heat. Conduction arises on a Ti sublattice via the t_{2g} orbitals with a narrow bandwidth (2 eV to 3 eV), displaying possible strong electronic correlations. The origin of the physics and electronic properties of the spinel structure are yet to be resolved. Our current research demonstrates the role of 3d electrons in the properties of LTO and LTVO. The full solid solution of LiTi$_{2-x}$V$_x$O$_4$ ($0 \leq x \leq 2$) has been investigated [24]. The replacement of V ions for Ti site modifies the bandgap and d electron/hole exchange in Ti energy levels in order to maintain electrical neutrality. Several mechanisms for understanding the quickly suppressed superconductivity with a slight doping of LTVO have been proposed. The slight doping of LTVO may incur two major electronic effects. The first one is a simple pair-breaking effect with electron spin $S = 1$ on superconductivity [20, 24]. The second one refers to the effect of carrier doping on electron correlation via band filling. The 3d electrons of V are assumed to hybridize the Ti conduction electrons, making them itinerant. A simple magnetic pair-breaking of electron spins induced by additional impurity is commonly assumed to be responsible for suppressing superconductivity based on the localized moments of 3d electrons of V [24]. The localized magnetic moment per V atom is estimated to be 1.7 μB in the V^{4+} state with $S = 1/2$ [24]. The XANES measurements at V K-edges plotted in Fig. 7 show that V is more likely to be in state 3+ (Bordage et al., 2110), which contains a d^2 electronic configuration and is supposed to offer a weak magnetic moment probably because of the antiparallel orientation of the electron spins. The decreased V magnetic moment is also obvious in LiZnV$_2$O$_4$ [35]. A second possible reason for a weak magnetic moment is the decreased charge carriers at Ti t_{2g} bands. In this case, V electrons are expected to be localized at the Ti conduction electrons. If the Ti ions in LTO possess oxidation numbers 3+ and 4+, then ~0.5 (t_{2g}) electrons are expected to be in the conduction band. This condition results in the observation of a d-d excitation within the energy range of 0 eV to 5 eV owing to the presence of electrons in the t_{2g} occupied state that are excited to either the t_{2g} or e_g unoccupied state. The number of electrons occupying the t_{2g} orbital is expected to decrease if the oxidation number of Ti increases from trivalence to quadrivalence because of the doping of V ions. The spectra in RIXS reveal a significant variation in the d-d excitation feature, which suggestively decreases when LTO becomes LTVO, even with slight doping of V ions. This situation shows the decreased Ti 3d occupied states with the increase of x concentration. The Ti t_{2g} occupation number is then altered upon V doping. This valence variation is small in XANES Ti K- or L-edges spectra, but weighty in RIXS spectra. The results, particularly the reflection of the decreased intensities of t_{2g}-t_{2g}, and t_{2g}-e_g transitions from the RIXS spectra,

support the role of these electronic states in rapidly suppressing T_c in slight V doping. Accordingly, the findings of this research support the conclusion that the decreased density of the states of Ti $3d$ electrons at E_F is responsible for rapidly suppressing superconductivity.
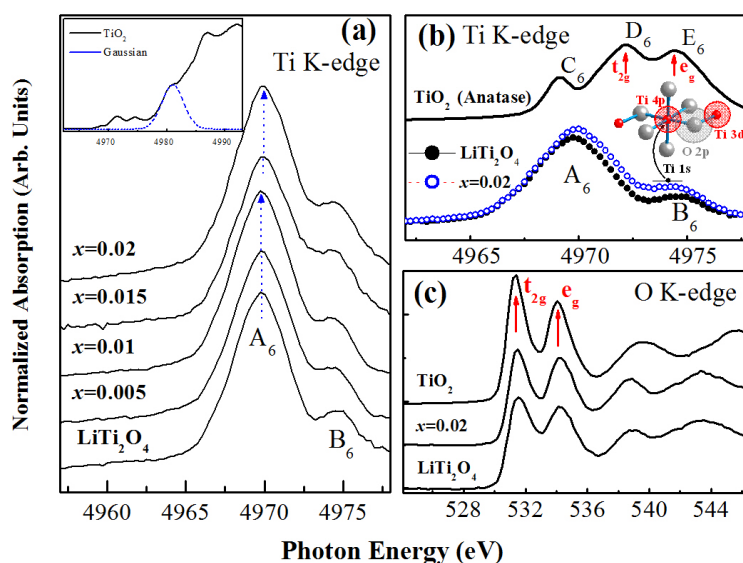
Figure 6. (a) XANES Ti K-edge spectra of LTVO (x = 0 to 0.2) and Anatase-TiO$_2$ in the pre-edge region. The inset shows that a Gaussian function was subtracted from the original TiO$_2$ spectrum. (b) Detailed comparison of the pre-edge region for LTO and LTVO (x = 0.02). (c) XANES O K-edge spectra shown with two main peaks in the pre-edge region corresponding to the hybridization of Ti $3d$ (t$_{2g}$ and e$_g$)-O $2p$ states.
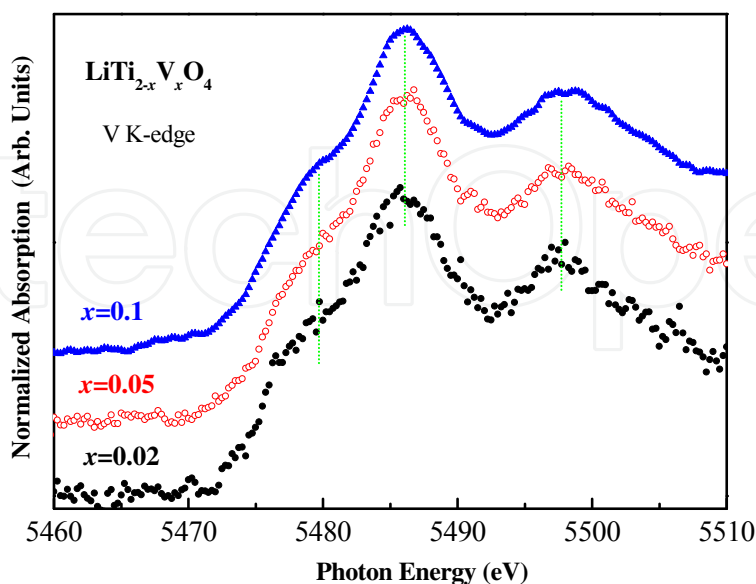
Figure 7. XANES V K-edge of LTVO (x = 0.02) compared with the larger doping of LTVO (x = 0.05 and 0.1). No significant variation is observed in the spectra

4. Conclusion

The results on the effect of V doping on the atomic and electronic structures of LTVO, XAS, and RIXS spectra reveal that the valence of V ions remains constant, but the hybridization of Ti-O considerably varies. In particular, the results show the mixed valency nature of Ti ions and a significant variation in the hybridization of Ti 3d-O 2p states. The sharp decrease in the superconductivity of V-doped samples is ascribed to the electron–orbital interaction arising from the hybridization of TM and O orbitals. Low-energy excitation because of d-d excitation indicates that electron correlation and Ti oxidation number are enhanced, which support the XAS observation. Meanwhile, the observed properties of superconductivity are attributed to an altered density of the states of Ti 3d electrons and Ti-O hybridization. The Ti electronic configuration and lattice distortion induce the rapidly suppressed superconductivity and are attributed to hybridization rather than to the magnetic nature of the substituted ion. This research also demonstrates that RIXS is a powerful tool for investigating the electronic states and electron correlations of Ti compounds, in which the XANES spectral features are subdued.

Author details

Chi-Liang Chen[1,2] and Chung-Li Dong[1,2]

1 Institute of Physics, Academia Sinica, Nankang, Taipei, Taiwan

2 National Synchrotron Radiation Research Center (NSRRC), Hsinchu, Taiwan

References

[1] Agui, A.; Uozumi, T.; Mizumaki, M. & Käämbra, T. (2009). Intermetallic charge transfer in FeTiO$_3$ probed by resonant inelastic soft x-ray scattering. *Physical Review B*, 79: 092402.

[2] Anisimov, V. I.; Korotin, M. A.; Zölfl, M.; Pruschke, T.; Hur, K. Le & Rice, T. M. (1999). Electronic Structure of the Heavy Fermion Metal LiV$_2$O$_4$. *Physical Review Letters*, 83: 364.

[3] Augustsson, A.; Henningsson, A.; Butorin, S. M.; Siegbahn, H.; Nordgren, J. & Guo, J.-H. (2003). Lithium ion insertion in nanoporous anatase TiO$_2$ studied with RIXS. *The Journal of Chemical Physics*, 119: 3983.

[4] Bordage, A.; Balan, E.; de Villiers, J. P. R.; Cromarty, R.; Juhin, A.; Carvallo, C.; Calas, G.; Sunder Raju, P. V. & Glatzel, P. (2011). V oxidation state in Fe–Ti oxides by high-energy resolution fluorescence-detected x-ray absorption spectroscopy. *Physics and Chemistry of Minerals*, 38: 449-458.

[5] Brydson, R.; Sauer, H.; Engel, W.; Thomass, J. M.; Zeitler, E.; Kosugi, N. & Kuroda, H. (1989). Electron energy loss and x-ray absorption spectroscopy of rutile and anatase: a test of structural sensitivity. *Journal of Physics: Condensed Matter*, 1: 797.

[6] Bussmann-Holder; Müller, K. A. & Keller, H. (2007). High T_c Superconductors and Related Transition Metal Oxides ISBN 3540710221.

[7] Cabaret, D; Bordage, A; Juhin, A; Arfaoui, M. & Gaudry, E. (2010). First-principles calculations of x-ray absorption spectra at the K-edge of 3*d* transition metals: an electronic structure analysis of the pre-edge. *Phys. Physical Chemistry Chemical Physics*, 12: 5619-5633.

[8] Cava, R. J.; Murphy, D. W.; Zahurak, S.; Santoro, A. & Roth, R. S. (1984). The crystal structures of the lithium-inserted metal oxides $Li_{0.5}TiO_2$ anatase, $LiTi_2O_4$ spinel, and $Li_2Ti_2O_4$. *Journal of Solid State Chemistry*, 53: 64-75.

[9] Chen, C. L. & Dong, C. L. (20012). SUPERCONDUCTOR-Materials, Properties and Applications, 2012 ISBN: 979-953-307-798-6 Chapter 2 'X-ray spectroscopy studies of the iron chalcogenides', 21-44.

[10] Chen, C. L.; Yeh, K. W., Huang, D. J., Hsu, F. C.; Lee, Y. C., Huang, S. W., Guo, G. Y.; Lin, H. J.; Rao, S. M. & Wu, M. K. (2008). Orbital polarization of the unoccupied states in multiferroic $LiCu_2O_2$. *Physical Review B*, 78: 214105.

[11] Dallera, C.; Grioni, M.; Shukla, A.; Vankó, G.; Sarrao, J. L.; Rueff, J. P. & Cox, D. L. (2002). New Spectroscopy Solves an Old Puzzle: The Kondo Scale in Heavy Fermions. *Physical Review Letters*, 88: 196403.

[12] De Groot, F. M. F.; Fuggle, J. C.; Thole, B. T. & Sawatzky, G. A. (1990). 2*p* x-ray absorption of 3d transition-metal compounds: A atomic multiplet descriptiom including the crystal field. *Physical Review B*, 42: 5459. (1990). $L_{2,3}$ x-ray-absorption edges of d^0 compounds: K^+, Ca^{2+}, Sc^{3+}, and Ti^{4+} in O_h (octahedral) symmetry. *Physical Review B*, 41: 928.

[13] De Groot, F. M. F.; Faber, J. C.; Michile, J. J. M.; Czyzyk, M. T.; Abbate, M. & Fuggle, J. C. (1993). Oxygen 1*s* x-ray absorption of tetravalent titanium oxides: A comparison with single-particle calculations. *Physical Review B*, 48: 2074

[14] Durmeyer, O.; Kappler, J. P.; Beaurepaire, E.; Heintz, J. M. & Drillon, M. (1990). TiK XANES in superconducting $LiTi_2O_4$ and related compounds. *Journal of Physics: Condensed Matter*, 2: 6127

[15] Finkelstein, L. D.; Zabolotzky, E. I.; Korotin, M. A.; Shamin, S. N.; Butorin, S. M.; Kurmaev, E. Z. & Nordgren, J. (2002). Vacant states of TiO_2 with rutile structure and their reflection in different-type x-ray absorption spectra. *X-ray Spectrometry*, 31: 414-418.

[16] Fazileh, F.; Gooding, R. J.; Atkinson, W. A. & Johnston, D. C. (2006). Role of Strong Electronic Correlations in the Metal-To-Insulator Transitionin Disordered $LiAl_yTi_{2-y}O_4$. *Physical Review Letters*, 96: 046410.

[17] Harada, Y.; Kinugasa, T.; Eguchi, R.; Matsubara, M.; Kotani, A.; Watanabe, M.; Yagishita, A. & Shin, S. (2000). Polarization dependence of soft-x-ray Raman scattering at the L edge of TiO$_2$. *Physical Review B*, 61: 12854.

[18] Hsu, F. C. Liao, Y. C.; Yan, D. C.; Gu, S. Y.; Wu, M. K.; Tang, H. Y. & Perng, T. P. (2007). Observation of metal–insulator transition in vanadium-doped superconducting Li(Ti$_{2-x}$V$_x$)O$_4$. *Physica C*, 460-462: 546-548.

[19] Hsu, F. C. (2009), Investigation of the electrical, magnetic and thermal properties of spinel LiTi$_{2-x}$M$_x$O$_4$ (M=V and Cr). Department of Materials Science and Engineering, *National Tsing Hua University, Taiwan.* Ph. D. Thesis.

[20] Itoh, Y,; Moritsu, N. & Yoshimura, K. (2008). Emergence of Antiferromagnetic Correlation in LiTi$_{2-x}$V$_x$O$_4$ via ^{7}Li NMR. *Journal of the Physical Society of Japan*, 77: 123713.

[21] Johnston, D. C. (1976). Superconducting and normal state properties of Li$_{1+x}$Ti$_{2-x}$O$_4$ spinel compounds. I. Preparation, crystallography, superconducting properties, electrical resistivity, dielectric behavior, and magnetic susceptibility. *Journal of Low Temperature Physics*, 25: 145-175

[22] Johnston, D. C.; Swenson,C. A. & Kondo, S. (1999). Specific heat (1.2–108 K) and thermal expansion (4.4–297 K) measurements of the 3*d* heavy-fermion compound LiV$_2$O$_4$. *Physical Review B*, 59: 2627.

[23] Joly, Y; Cabaret, D.; Renevier, H. & Natoli, C. R. (1999). Electron Population Analysis by Full-Potential X-Ray Absorption Simulations. *Physical Review Letters*, 82: 2398.

[24] Kichambare, P. Kijima, N.; Honma, H., Ebisu, S. & Nagata, S. (1996). Suppression of superconductivity in Li(Ti$_{1-x}$V$_x$)$_2$O$_4$. *Journal of Physics and Chemistry of Solids*, 57: 1615-1620.

[25] Kucheyev, S. O.; van Buuren, T.; Baumann, T. F.; Satcher, J. H.; Willey, Jr., T. M.; Meulenberg, R. W., Felter, T. E.; Poco, J. F.; Gammon, S. A. & Terminello L. J. (2004). Electronic structure of titania aerogels from soft x-ray absorption spectroscopy. *Physical Review B*, 69: 245102.

[26] Lambert, P. M.; Edwards, P. P. & Harrison, M. R. (1990). Magnetism, superconductivity, and the metal-nonmetal transition in the spinel LiM$_x$Ti$_{2-x}$O$_4$; M = Al^{3+}, Cr^{3+}. *Journal of Solid State Chemistry*, 89: 345-360.

[27] Lytle, F. W., Greegor, R.B., Sandstrom, D.R., Marques, E.C., Wong, J., Spiro, C.L., Huffman, G.P. & Huggins, F. E. (1984). Measurement of soft x-ray absorption spectra with a fluorescent ion chamber detector. Nuclear Instruments and Methods in Physics Research Section A: Accelerators, Spectrometers, Detectors and Associated Equipment, 226:542-548.

[28] Le Fèvre, P.; Danger, J.; Magnan, H.; Chandesris, D.; Jupille, J.; Bourgeois, S.; Arrio, M. A.; Gotter, R.; Verdini, A. & Morgante, A. (2004). Stoichiometry-related Auger

lineshapes in titanium oxides: Influence of valence-band profile and of Coster-Kronig processes. *Physical Review B*, 69: 155421.

[29] Lide, D. R. (2007-2008) CRC handbook of Chemistry and Physics, 88th edition, Taylor & Francis Group.

[30] Maddox, B. R.; Lazicki, A.; Yoo, C. S.; Iota V.; Chen, M.; McMahan, A. K.; Hu, M. Y.; Chow, P.; Scalettar, R. T. & Pickett, W. E. (2006). 4f delocalization in Gd: Inelastic x-ray scattering at ultrahigh pressure. *Physical Review Letters*, 96: 215701.

[31] Matsubara, M.; Uozumi, T.; Kotani, A.; Harada, Y. & Shin, S. (2002). Polarization dependence of resonant x-ray emission spectra in $3d^n$ transition metal compounds with n = 0, 1, 2, 3. *Journal of the Physical Society of Japan*, 71: 347-356.

[32] Massidda, S.; Yu, J. & Freeman, A. J. (1988). Electronic structure and properties of superconducting $LiTi_2O_4$. *Physical Review B*, 38: 11352.

[33] Merz, M.; Nücker, M.; Schweiss, P.; Schuppler, S.; Chen, C. T.; Chakarian, V.; Freeland, J.; Idzerda, Y. U,; Kläser M.; Müller-Vogt, M. & Wolf, Th. (1998). Site-Specific X-Ray Absorption Spectroscopy of $Y_{1-x}Ca_xBa_2Cu_3O_{7-y}$: Overdoping and role of apical oxygen for high temperature superconductivity. *Physical Review Letters*, 80: 5192.

[34] Millis, A. J. (1998). Lattice effects in magnetoresistive manganese perovskites. *Nature*, 392: 147.

[35] Muhtar; Takagi, F.; Kawakami, K. & Tsuda, N. (1988). Magnetic Susceptibility of Metal-Insulator System $Li_xZn_{1-x}V_2O_4$. *Journal of the Physical Society of Japan*, 57: 3119-3127.

[36] Nordgren, J.; Bray, G.; Cramm, S.; Nyholm, R.; Rubensson, J. E. & Wassdahl, N. (1989). Soft x-ray emission spectroscopy using monochromatized synchrotron radiation (invited). *Review of Scientific Instruments*, 60: 1690.

[37] Poumellec, B.; Marucco, J. F. & Touzelin, B. (1987). X-ray-absorption near-edge structure of titanium and vanadium in $(Ti,V)O_2$ rutile solid solutions. *Physical Review B*, 35: 2284.

[38] Parlebas, J. C.; Khan, M. A.; Uozumi, T.; Okada, K. & Kotani, A. (1995). Theory of many-body effects in valence, core-level and isochromat spectroscopies along the $3d$ transition metal series of oxides. *Journal of Electron Spectroscopy and Related Phenomena*, 71: 117.

[39] Ra, W.; Nakayama, M.; Uchimoto, Y. & Wakihara, M. (2005). Experimental and computational study of the electronic structural changes in $LiTi_2O_4$ Spinel Compounds upon Electrochemical Li insertion reactions. *The Journal of Physical Chemisity B*, 109(3): 1130-1134.

[40] Richter, J. H.; Henningsson, A.; Sanyal, B.; Karlsson, P. G.; Andersson, M. P.; Uvdal, P.; Siegbahn, H.; Eriksson, O. & Sandell, A. (2005). Phase separation and charge localization in UHV-lithiated anatase TiO$_2$ nanoparticles. *Physical Review B*, 71: 235419.

[41] Rotter, M,; Tegel, M. and Johrendt, D. (2008). Superconductivity at 38 K in the Iron Arsenide (Ba$_{1-x}$K$_x$)Fe$_2$As$_2$. *Physical Review Letters*, 101: 107006.

[42] Rueff, J. P.; Hague, C. F.; Mariot, J. M.; Journel, L.; Delaunay, R.; Kappler, J. P.; Schmerber, G.; Derory, A.; Jaouen, N. & Kril,l G. (2004). f-state occupancy at the γ-α phase transition of Ce-Th and Ce-Sc alloys. *Physical Review Letters*, 93: 067402.

[43] Sun, C. P.; Lin, J. Y.; Mollah, S.; Ho, P. L.; Yang, H. D.; Hsu, F. C.; Liao, Y. C. & Wu, M. K. (2004). Magnetic field dependence of low-temperature specific heat of the spinel oxide superconductor LiTi$_2$O$_4$. *Physical Review B*, 70: 054519.

[44] Uozumi, T.; Okada, K.; Kotani,; Durmeyer, A. O.; Kappler, J. P.; Beaurepaire, E. & Parlebas, J. C. (1992). Experimental and Theoretical Investigation of the Pre-Peaks at the Ti K-Edge Absorption Spectra in TiO$_2$. *EPL (Europhysics Letters)*, 18: 85.

[45] Warwick, T.; Heimann, P.; Mossessian, D.; McKinney, W. & Padmore, H. (1995). Performance of a high resolution, high flux density SGM undulator beamline at the ALS (invited). *Review of Scientific Instruments*, 66: 2037.

[46] Wu, Z. Y.; Ouvrard, G.; Gressier, P. & Natoli, C. R. (1997). Ti and O K edges for titanium oxides by multiple scattering calculations: Comparison to XAS and EELS spectra. *Physical Review B*, 55: 10382.

[47] Xiao, G.; Cieplak, M. Z.; Xiao, J. Q. & Chien, C. L. (1990). Magnetic pair-breaking effects: Moment formation and critical doping level in superconducting La$_{1.85}$Sr$_{0.15}$Cu$_{1-x}$A$_x$O$_4$ systems (A=Fe, Co, Ni, Zn, Ga, Al). *Physical Review B*, 42: 8752(R)

[48] Xiao, G.; Streitz, F. H.; Gavrin, A.; Du, Y. W. & Chien C. L.(1987). Effect of transition-metal elements on the superconductivity of Y-Ba-Cu-O. *Physical Review B*, 35: 8782(R)

[49] Xu, F.; Liao, Y. C.; Wang, M. J.; Wu, C. T.; Chiu, K. F. & Wu, M. K. (2003). The Preparation Effect of Li$_{1+x}$Ti$_2$O$_4$ and Its Aging Effect. *Journal of Low Temperature Physics*, 131: 569-574.